This is a previous version of the article published in IEEE Transactions on Antennas and Propagation. 2018, 66(8): 3837-3845. doi:10.1109/TAP.2018.2835639

Single-Layer Circularly-Polarized Ka-Band Antenna using Gap Waveguide technology

Miguel Ferrando-Rocher, *Student Member, IEEE,* Jose I. Herranz-Herruzo, *Member, IEEE,* Alejandro Valero-Nogueira, *Member, IEEE,* Antonio Vila-Jiménez

***Abstract*—A single-layer circularly-polarized array antenna is proposed in the context of the so-called Gap Waveguide Technology. This ultra-compact antenna combines the corporate-feeding network, the radiating apertures and the polarizer over one single layer, standing out among solutions proposed so far in this technology. Apertures are fed through a corporate feeding network combining both Groove and Ridge Gap Waveguides and backed by chamfered cylindrical cavities. Such cavities are naturally integrated within the bed of nails hosting grooves and ridges, leading to a very low-profile 4×4 array. Experimental results are presented to confirm the good radiation performance reported by simulations. The proposed array architecture may be seamlessly enlarged to any size thanks to the scalability of the gap-based corporate feeding network, making this solution very attractive for medium to high-gain applications.**

***Index Terms*—Gap Waveguides, aperture array, Single-layer, Ka-band, Ridge Gap Waveguide, Groove Gap Waveguide, Circular polarization**

I. Introduction

On-the-move Satellite Communications (SOTM) is currently a market of growing interest. Antennas for applications in this field are subject to very challenging specifications, being the size one of them. Compact low-profile antennas, able to be mounted in all types of vehicles, from airplanes to trains or ground vehicles, are very welcome. Low cost and weight are among the targets as well. These good physical properties, of course, must not impede the compliance with tough electrical specifications in terms of beam quality, high gain and low cross-polarization in order to highly concentrate on the communication object [1]. Moreover, recent satellite communication systems are increasing its operation frequency from Ku to Ka band [2] and the circular polarization has been widely adopted. Bringing together all these specifications, new solutions must not only attain the electric performance of Ku-band antennas currently in use, but also exhibit added values in terms of polarization, lightness, volume and cost at the demanding 30 GHz band.

As we have seen, there are different technologies and research lines open to satisfy these requirements. One technology that can meet some of those needs is Gap Waveguide Technology (GW) [3]. This technology is very appealing for millimeter-wave band because it enables fully-metallic distribution networks in a much simpler way than conventional waveguides. Very low distribution losses can be achieved while partially retaining the assembly simplicity of multi-layer microstrip feeding networks. This unique feature is a consequence of gap waveguides ability to safely confine the electromagnetic wave propagation through a contactless structure.

This work was supported by the Spanish Ministry of Economics and competitiveness under projects TEC2013-47360-C3-3-P and TEC2016-79700-C2-1-R.

M. Ferrando-Rocher, J. I. Herranz-Herruzo, A. Valero-Nogueira, and A. Vila-Jiménez are with the Instituto de Telecomunicaciones y Aplicaciones Multimedia (ITEAM) of the Universitat Politècnica de València, c/ Cami de Vera s/n, 46022 Valencia, Spain (e-mail: miferroc@iteam.upv.es, jiherhe@upvnet.upv.es, avalero@dcom.upv.es, anviji@upv.es)

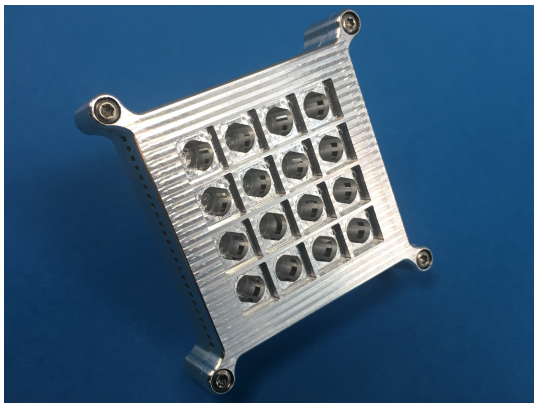

Fig. 1: Perspective view of the manufactured antenna.

During the last decade there have been important advances in this technology and a good number of gap waveguide-based arrays can be found. Gap waveguides were introduced by the late professor P.-S. Kildal who patented the concept. These waveguides are formed out of two parallel plates. One is a conducting flat plate while the other is textured with a bed of nails [3]. Such textured surface creates a high-impedance condition, which ideally emulates the behaviour of a perfect magnetic conductor (PMC) for a given frequency band. If the air gap between the parallel plates is smaller than a quarter of wavelength, the combination of the two boundary conditions establishes a cut-off condition. Therefore, propagation of all parallel-plate modes is forbidden within a certain frequency band. Only if a groove or a ridge is inserted among the nails, wave propagation can take place. In the first case the transmission media is called groove gap waveguide (GGW), while in the second the guided wave follows a ridge gap waveguide (RGW) [4], [5], [6]. In recent years this technology has demonstrated to be a good candidate for antennas and even filters with very low insertion losses. Two successful examples of low-loss filters using Gap Waveguides are presented in [7] and [8]. Both filters were successfully designed and measured

at V band, where tolerances are far more critical than in Ka band. For the sake of illustration only, remarkable insertion losses around 1.5 dB were experimentally obtained for both devices.

Most of the array instances found in the recent gap waveguide literature radiate linear polarization and resort to a multilayer scheme to reach all radiating slots. In [9], three metal layers are piled up in a conventional fashion, i.e., feed network, coupling layer and radiating layer. No need to assess good electrical contact between them was required, thanks to the gap waveguide properties.

To a much lesser extent, there have also been attempts to deal with circularly polarized arrays fed by gap waveguides. In [10], a 1 4 array fed by RGW was presented. However, that topology is not easily extendable to a 2-D arrangement without grating lobes appearing in radiation patterns. Note that in this case larger spacing between radiating elements would be required to allow feed branches to pass among them.

In this context, the authors proposed in [11] a new concept that combines RGW and GGW waveguides within the same network to attain a very compact array feeding topology. Such concept is used here to fit the feeding network into the same layer as the circularly polarized radiating elements, giving rise to a single-layer array. In this regard, such topology recalls the conventional microstrip patch arrays, in the sense that patches and corporate network share the same surface. Microstrip technology is a mature and versatile technology. Numerous examples can be found in the literature about microstrip array antennas fed by corporate networks, either with linear or circular polarization. Those antennas, however, are not suitable for high gain applications at the target frequency band since losses increase dramatically with array size. That is the main reason why waveguide-based networks are preferred. In this case, though, shielding issues become a major concern.

Gap waveguides come to bridge the gap between those approaches: far less lossy than microstrip technology but retaining its handling simplicity. A detailed study comparing losses of these three technologies, RW, microstrip and gap waveguides in the mm-waveband was done in [12]. There, it is shown that, although losses in rectangular waveguide are the lowest, those of gap waveguide keep close to them and are considerably lower than those of microstrip or SIW.

Lastly, the manufacturing technique known as *Diffusion bonding* has also been shown to be an effective technology to assemble full-metallic high-gain multilayer antennas in the mm-wave band. Valuable examples for linear and dual-polarized antennas are detailed in [13] and [14], respectively. Typical handicaps for this technology, though, remain its complexity and relatively high cost. It seems, however, that its use is spreading and it could become a competitive technology in medium term, especially for V-band arrays.

The work presented here intends to provide solutions to some of the challenges described above by proposing a single-layer array solution, easily expandable to any size. A 4 4 Ka-band single-layer circularly-polarized array, shown in Fig. 1, has been designed and constructed. Such array is composed of chamfered cylindrical radiating apertures fed by a corporate gap-waveguide network. The rest of the paper is put forth as follows. In Section II, the basic radiating element of the array is presented. Section III is focused on the combined Ridge-Groove gap-waveguide distribution network. Section IV describes the 4 4 array design, leaving Section V for the experimental validation in terms of one fabricated prototype.

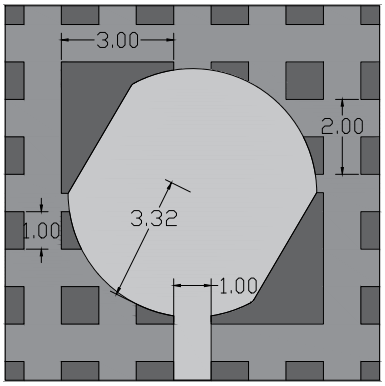

Fig. 2: Top view of the basic radiating element. The main dimensions are indicated in millimeters. Nails are colored in the darkest gray and the groove in the clearest one.

II. Basic radiating element

The basic radiating element is shown in Fig. 2. It is an open chamfered circular waveguide with a short in the back. The diameter is such that the waveguide is above cutoff in the desired frequency range. The aperture is fed by a groove gap waveguide [15] coming from its side to a point such that two orthogonal modes in quadrature are excited. In a previous work [16], the authors already presented this kind of open-ended waveguide as the basic radiating element for a dual linearly-polarized array in V-band. That idea has been extended here to radiate circular polarization in a single-layer configuration. The design of these chamfers as well as an overview of thes unit cell are described below.

The bed of nails, as shown in Fig. 2, surrounds both the aperture and the feeding groove. These nails are responsible for keeping the electromagnetic field confined within the feeding waveguides and radiating cavities in a contactless fashion. Therefore, it is important to determine the proper dimensions of nail height and width, h_p and l_p, respectively, as well as nail periodicity, p_p. Such periodic structure must exhibit its cutoff properties at the targeted band, from 29.5 GHz to 31 GHz. Optimized dimensions are found to be $h_p = 2.5$ mm, $l_p = 1$ mm and $p_p = 2$ mm. Fig. 3 shows the attained band-gap performance, ranging from 22 GHz to 53 GHz, which broadly covers the required frequency range. This is certainly far more bandwidth than necessary, but it can also be convenient. A wider stopband may be advantageous if, for example, a frequency shift occurs due to inaccuracies in nails manufacturing. In such case the working frequency band would still be within the structure's stopband.

The relevant design parameters regarding the stopband bandwidth are the nail height, the periodicity between nails and the air gap height. Nail width affects also the bandwidth but it plays a minor role. Note that wide nails would make the

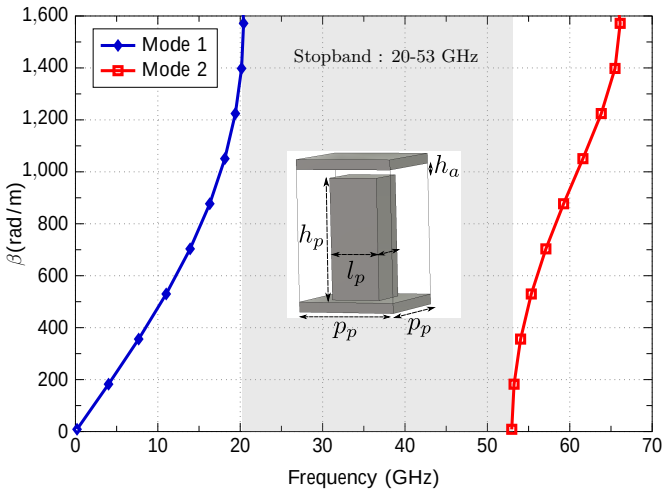

Fig. 3: Dispersion diagram of the bed of nails using the following dimensions: h_p = 2.5 mm, l_p = 1 mm and p_p = 2 mm. Stopband is generated from 20 GHz to 53 GHz, enough for covering the band of interest in this work (29.5 GHz to 31 GHz).

antenna less compact and radiating elements might be spaced beyond λ_o, whereas narrow nails increase the fabrication complexity. A compromise width value has been chosen. On the other hand, around the array and network, four rows of nails have been arranged for isolation purposes. Three rows would already provide 60 dB of isolation, which is considered enough for most applications. Here, four rows have been used just to get rid of any source of uncertainty coming from the experimental results, given that we are dealing with a new type of antenna.

Once the bed of nails is designed, a proper feeding network topology, capable of accessing a two-dimensional array of radiating elements, must be arranged. Two main requirements have determined the solution. Firstly, a corporate topology has been assumed in order to maximize the operation bandwidth. This decision seriously conditions the second requirement: the feeding network must share the layer with the radiating elements to meet the low-profile specification. These considerations and the adopted solutions are detailed in the next section.

III. Combined Ridge-Groove Gap Waveguide Distribution Network

In the context of Gap Waveguide Technology, E-plane GGW corporate topologies provide very compact networks since the groove can be made much narrower than its H-plane counterpart. Such type of network was already used for a 4 4 slot array in [17] but some tricks had to be introduced to compensate for the well-known phase inversion at the E-plane splitter outputs, which in turn led to an asymmetric configuration. Conversely, the distribution network could also be realized in RGW [18] to avoid such phase inversion. RGW propagation channel, however, generally requires more room than the GGW one, forcing larger spacing between the arrayed radiators. Therefore, grating lobes will be difficult

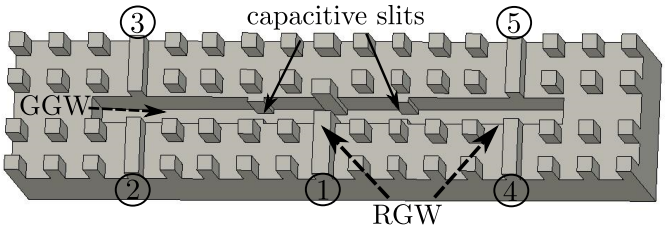

Fig. 4: Geometry of the proposed 1:4 RGR power divider.

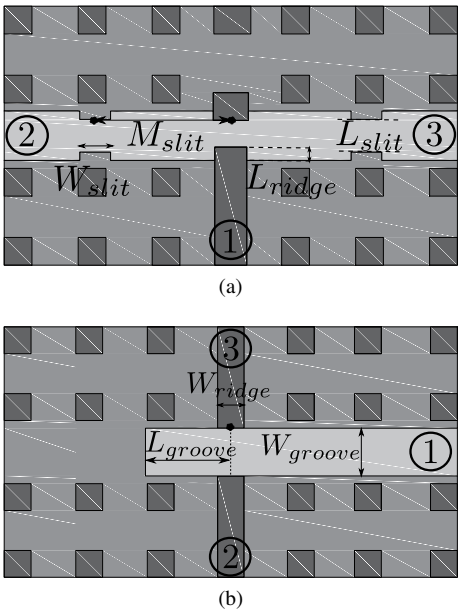

(a)

(b)

Fig. 5: 1:2 power divider, from ridge to groove, is shown in (a). Input port is located in the ridge and output ports are in the grooves. In (b) the inverse case is shown. Input port is in the groove while the output ports are in the ridges. The legend with the design parameters is inset. The optimized values for each parameter are collected in Table I.

to avoid. These two difficulties can be solved when GGW and RGW are conveniently combined together as part of the same distribution network [11]. To do so, each power splitting entails also a switch in waveguide type, from RGW to GGW and vice versa, as shown in Fig. 4. This waveguide combination naturally removes the undesired phase inversion and halves the presence of wider RGW waveguides. Let us remark in passing that this sort of versatility is linked to the contactless nature of these waveguides and is one of the nice properties associated to gap waveguides.

Let us observe each divider separately. Ridge-to-groove (RG) divider is shown in Fig. 5a. Notice that the ridge protrudes slightly into the groove to help the necessary 90 rotation of the electric field from ridge to groove. Fig. 6 shows how this rotation occurs quite naturally in the transition. In addition, capacitive slits can be created in the groove to improve matching. Protrusion depth and slit parameters need to be optimized to get the most out of the transition.

Groove-to-ridge (GR) divider is singled out in Fig. 5b. Ridges meet the groove at $\lambda_g/4$ from the groove backshort so that the transverse component of the electric field is at a

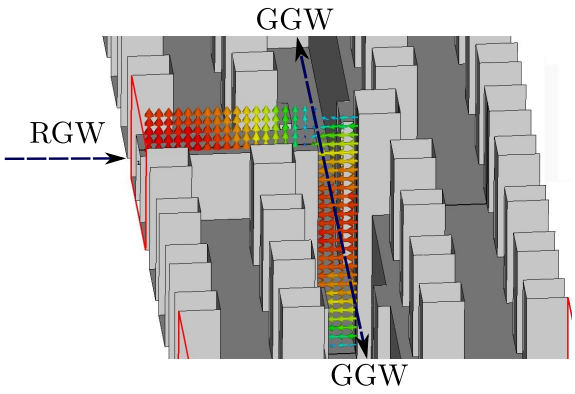

Fig. 6: Electrical field representation at the discontinuity between RGW and GGW.

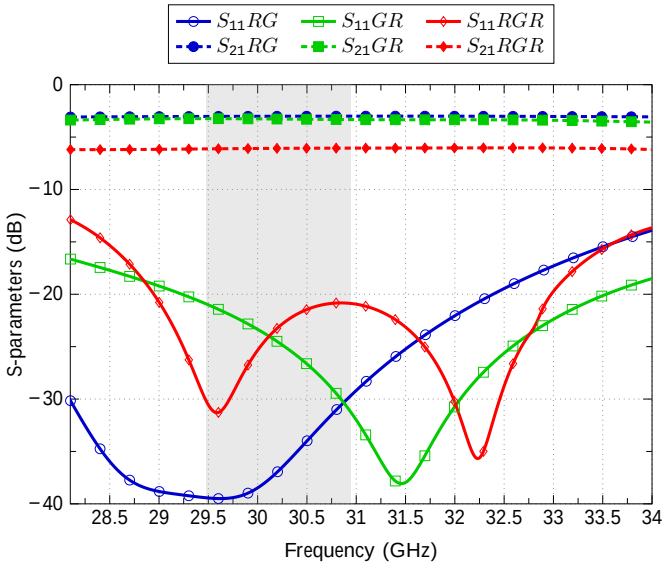

Fig. 7: S-parameters vs. frequency for the designed RG, GR and RGR dividers. The frequency band of the antenna is shaded.

maximum. Notice that there is no ridge protrusion here (as in RG divider) and in fact it has been observed that such protrusion here would deteriorate the overall divider performance. Fig. 7 shows reflection coefficient and insertion loss for both RG and GR dividers within a wide frequency range. The combined effect of both dividers in a Ridge-Groove-Ridge (RGR) fashion is evaluated also in Fig. 7, providing the S-parameters of the 1:4 divider depicted in Fig. 4. Performance is similar to that of the dividers alone and good enough for an array distribution network. In the 1:2 dividers, a flat S_{n1} ($n = 2, 3$) of 3 dB is obtained, while for the RGR, the S_{n1} ($n = 2, 3, 4, 5$) is 6 dB as expected from a 1:4 divider. Notice that the impedance bandwidth is much wider than specified for this application. The designed RGR divider manifests return losses better than 20 dB within a relative frequency bandwidth around 13%, from 29 to 33 GHz. All dimensions involved in the dividers optimization are shown in Table I. As remarked earlier, the proper combination of gap waveguides provides the desired in-phase uniform distribution at the four divider outputs.

TABLE I: Design parameters of the RGR network.

RGW dimensions		*Slit dimensions*		*GGW dimensions*	
W_{ridge}	0.80 mm	W_{slit}	1 mm	W_{groove}	1.5 mm
L_{ridge}	0.43 mm	L_{slit}	1 mm	L_{groove}	2.4 mm
H_{ridge}	1.57 mm	M_{slit}	4.4 mm	H_{groove}	3.4 mm

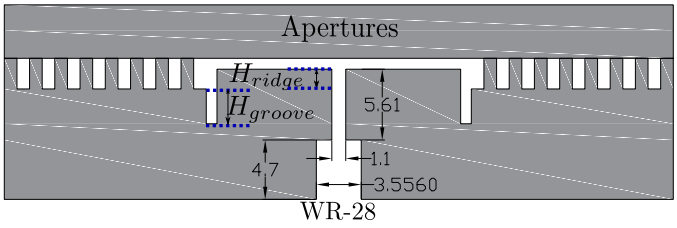

Fig. 8: Cross-sectional side view of the 4 4 antenna. A complete view from the WR-28 input port to the first GGW, passing through the input RGW, can be seen. Most relevant dimensions of the WR-28 to RGW transition are shown.

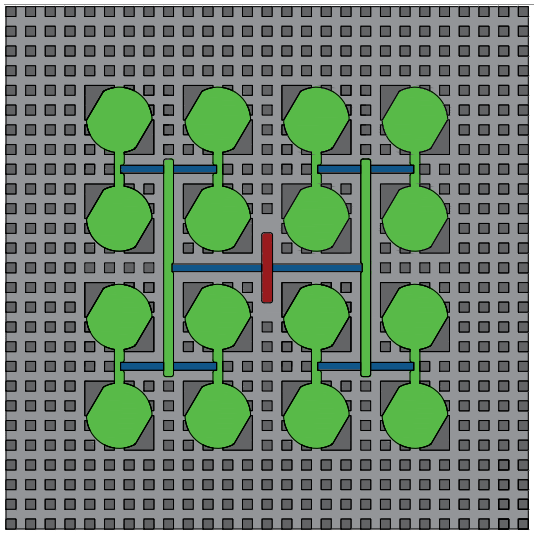

Fig. 9: Layout of the 4 4 antenna. The 2.5 mm high nails are colored in dark gray, the Ridge Gap Waveguide in blue, the Groove Gap Waveguide in green and the input waveguide in red. The total size of the antenna is about 53 53 mm^2.

IV. Array Design

The basic radiating element and the feed network described in previous sections are put together here to build a 4 4 array. The size chosen is considered large enough to demonstrate how these two structures can be combined in an array, being the extension to larger arrays formally straightforward. The apertures are uniformly spaced and surrounded by the corporate feeding network combining RGW and GGW.

The antenna input is located at the back surface with a transition to a WR-28 standard waveguide port. The lack of room left by the corporate network and the apertures forced us to excite the RGW by a reduced cross-section waveguide. Hence, a stepped transition to a WR-28 waveguide has been designed separately. It is found that one single step is enough to achieve good impedance matching. A cross-sectional view

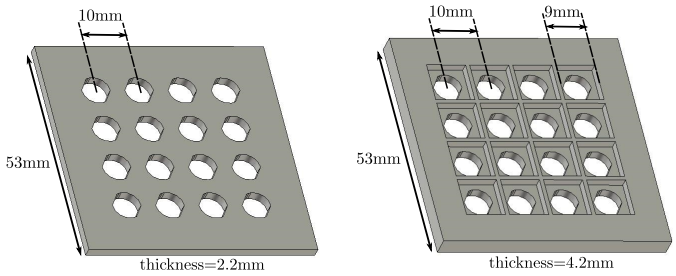

(a) (b)

Fig. 10: (a) Antenna lid showing the chamfered apertures. (b) Antenna lid with the waffle grid framing the original apertures.

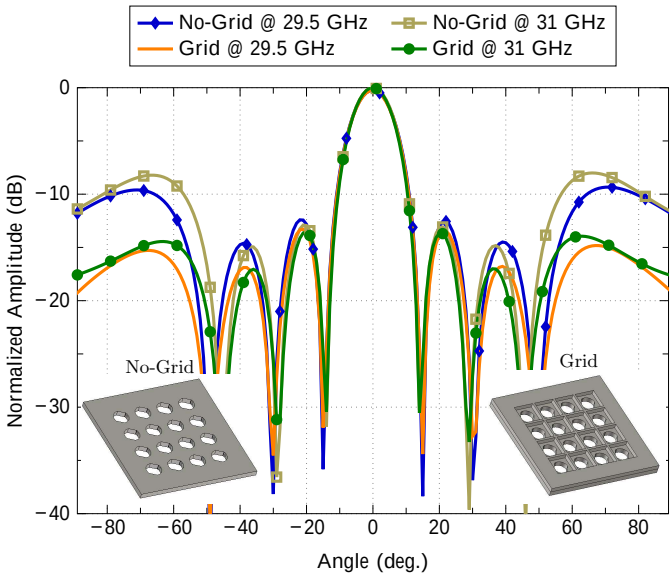

Fig. 11: Radiation patterns with and without grid. Patterns are at the lower and upper frequency of the band (XZ-plane).

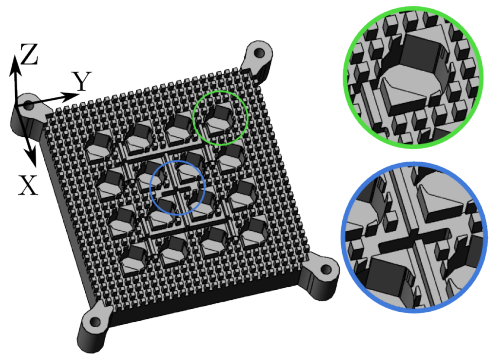

Fig. 12: 3D model of the 4 4 antenna. Detailed views of one cavity and the input are enlarged.

of the transition from WR-28 standard waveguide to RGW is shown in Fig. 8 and a front view in Fig. 9.

A. *Waffle grid*

Given the size of the chamfered holes and the room required by the waveguide feeding network within the bed of nails

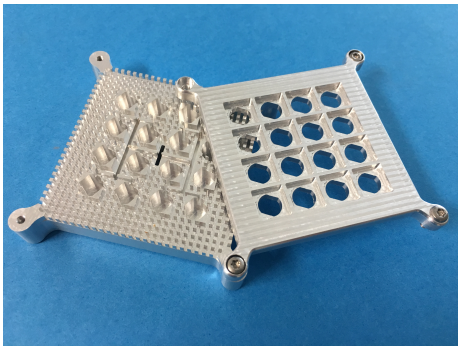

Fig. 13: Antenna array prototype.

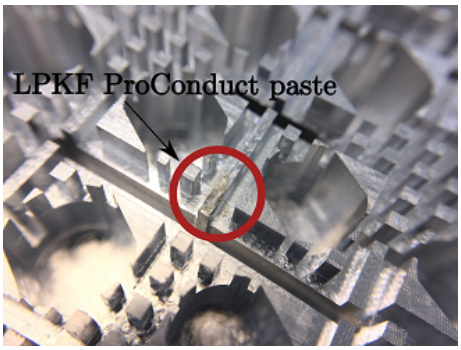

Fig. 14: Picture of the RGW where the drilled hole has been covered by the LPKF ProConduct paste.

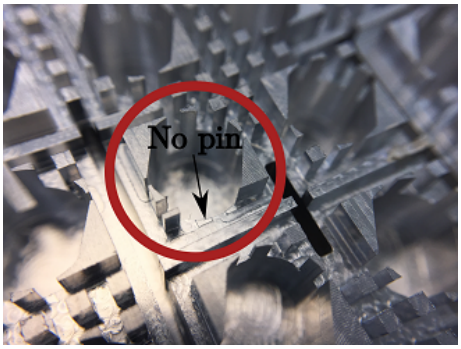

Fig. 15: Detail of the sector where a nail was incorrectly milled out.

environment, the apertures have been spaced as close as possible, i.e., 10 mm in our case, as illustrated in Fig. 10a. Such array spacing corresponds to $1.03\lambda_0$ at the maximum frequency of the intended band, 31 GHz, therefore grating lobes will still be present. To alleviate their effect, a waffle grid has been added to the lid. The waffle grid frames each chamfered aperture into a larger square one, as depicted in Fig. 10b. If a proper waffle height is chosen, both fundamental degenerate modes are properly excited at the square apertures. Hence, such grid preserves the circular polarization while increasing the effective aperture area. This field *filling* effect at the aperture level leads to a significant reduction in grating lobes level, as shown in Fig. 11. Sidelobes at $\theta = 70$ are lowered by more than 5 dB. Notice that the thickness of the waffle grid itself is 2 mm only, a reasonable value in terms of

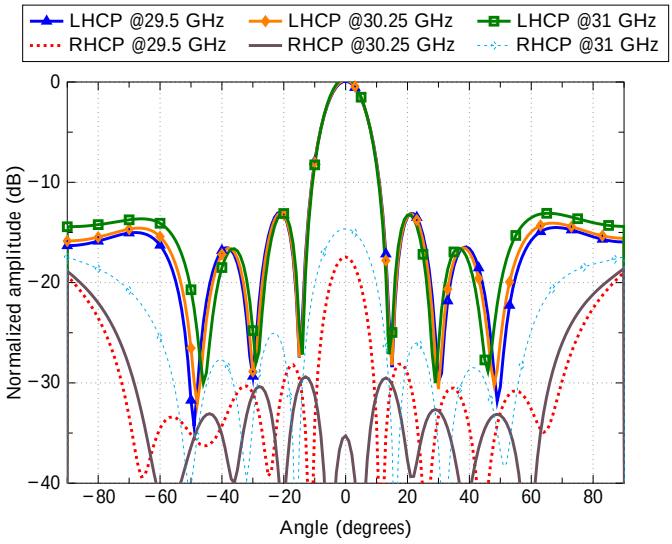

Fig. 16: Copolar and cross-polar simulated radiation patterns (YZ-plane) at several frequencies.

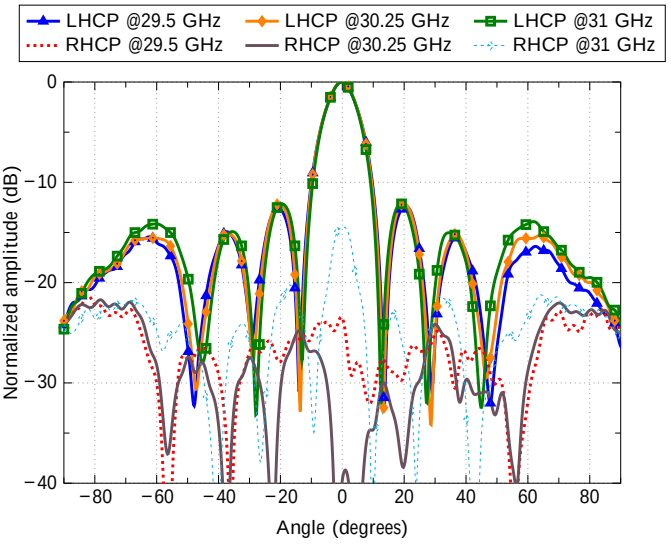

Fig. 18: Copolar and cross-polar measured radiation patterns (YZ-plane) at several frequencies.

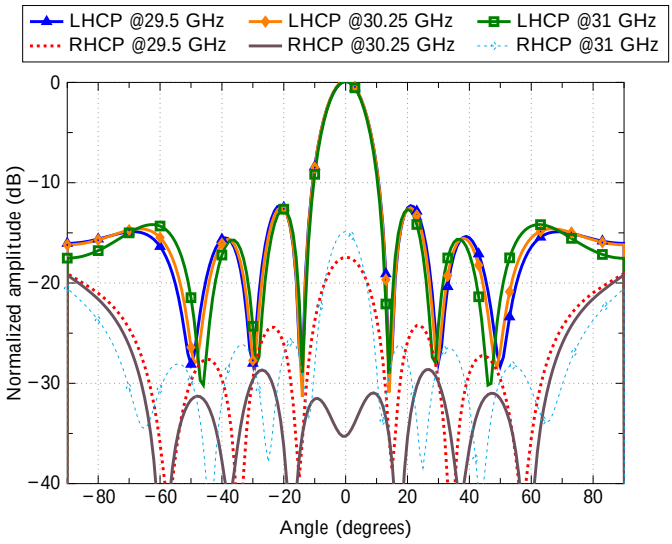

Fig. 17: Copolar and cross-polar simulated radiation patterns (XZ-plane) at several frequencies.

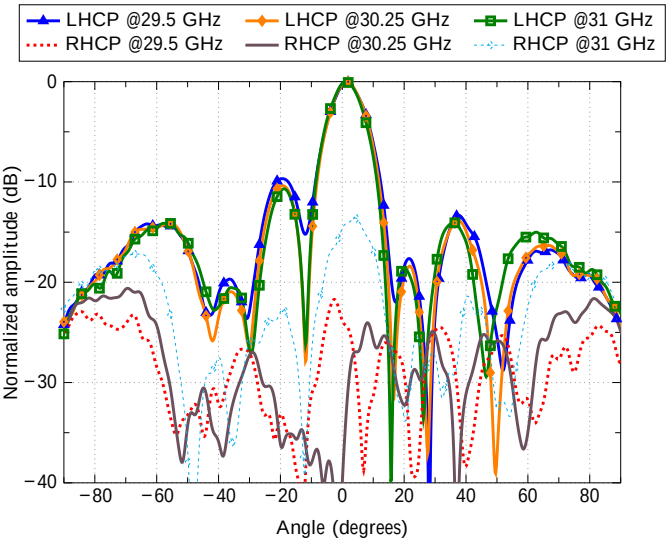

Fig. 19: Copolar and cross-polar measured radiation patterns (XZ-plane) at several frequencies.

total antenna height.

B. Manufacturing process

The antenna has been fully manufactured and measured in-house. Fig. 12 shows the final 3D layout before manufacturing. Input section and one of the cavities have been zoomed in for clarity. The fabricated antenna is shown in Fig. 13, where the two pieces have been disassembled to uncover the bottom one. For manufacturing, a Datron M-25 CNC Milling Machine has been used. Machine tolerances and milling restrictions influenced some of the dimensions finally chosen. In particular, groove depth and width are constrained by the milling tools available. Notice that the deeper the groove, the wider the tool must be. Grooves cannot be made as deep and narrow as one would wish. Given the operation band, a groove depth of at least 6 mm (h_p+ H_{groove}) is required, which forced us to use a milling tool of 0.4 mm in diameter. Thicker tools would damage groove walls due to unavoidable vibrations.

Despite these fabrication precautions, a couple of errors during milling were detected. The first one was caused by inconsistencies of the CNC Milling Machine while the other can be attributed to a milling software bug. The most serious one was a hole perforated onto one of the input ridges. It was decided to try to fix this pitfall by filling the wrong drilling in with a conducting paste (LPKF ProConduct). Fig. 14 shows the fixed hole, covered by the paste. The second error detected was related to a missing nail in one of the cavities, apparently swept away by the machine. In Fig. 15 it can be seen that the tool overdrilled a metallic part between the input ridge and one cavity, removing one nail and part of the cavity chamfer. Since only one row of nails is used to isolate the ridge from the cavities, this nail plays a key role. Unfortunately, this

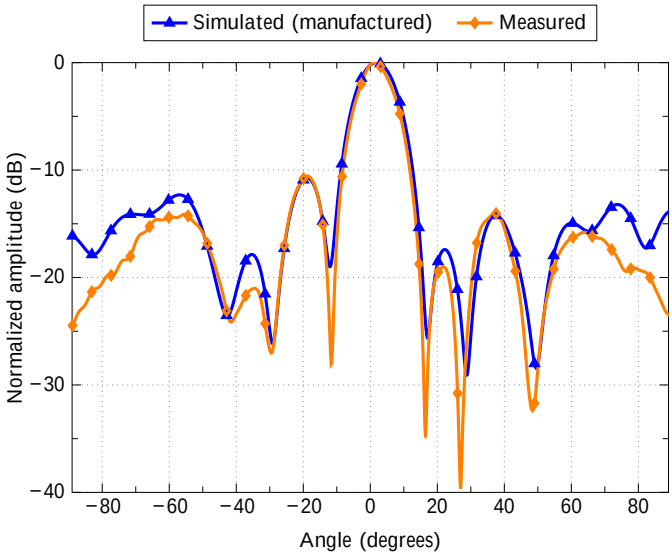

Fig. 20: Copolar radiation pattern (XZ-plane) at 31 GHz including the machining errors in simulation.

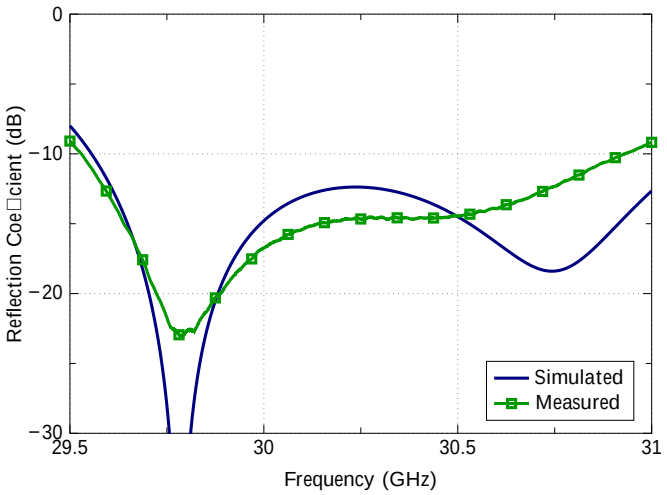

Fig. 21: Measured and simulated reflection coefficient versus frequency.

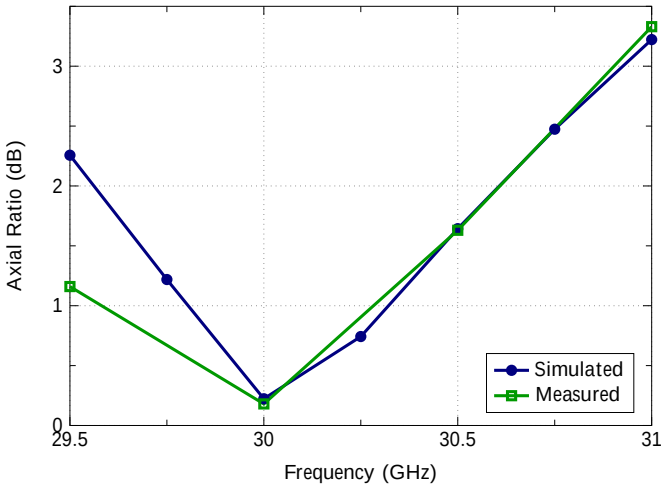

Fig. 22: Measured and simulated axial ratio versus frequency.

error could not be fixed and its effect will reveal as pattern asymmetries along the XZ plane.

V. Experimental Results

The fabricated prototype was subject to a measurement campaign at several sampled frequencies within the band. For the sake of comparison, simulated copolar and cross-polar radiation patterns are first shown in Figs. 16 and 17. These graphs represent $\phi = 90$ and $\phi = 0$ cuts, respectively. As can be observed, both cuts reveal an excellent stability versus frequency. First sidelobes appear at 13 dB level, as can be expected from a uniform illumination. Measured radiation patterns in the main cuts are shown in Figs. 18 and 19. Remarkable agreement between simulations and measurements can be noticed along YZ-plane ($\phi = 90$). XZ-plane, conversely, reveals a clear asymmetry which can be attributed to the manufacturing errors discussed above.

To prove the statement above further, the antenna has been resimulated including the machining errors detected. Fig. 20 shows now a much better agreement between measurements and simulations for XZ-plane. Although it is difficult to quantify exactly the amount of badly milled metal, the estimation clearly demonstrates the cause behind the asymmetry along this pattern cut.

Fig. 21 plots the measured S_{11}-parameter for the band of interest. It remains below 10 dB as predicted by simulations. With respect to the circular polarization purity, measured and simulated axial ratio are shown in Fig. 22. Nearly ideal 0-dB axial ratio has been sampled at 30 GHz, rising up to 1 dB and 3 dB for the lower and upper band edges, respectively. Satisfactory agreement with simulations can be noticed, being measurements even better in the lower part of the band. Nevertheless, notice that values below 3 dB could be obtained just by a slight design re-tuning toward higher frequencies. Such re-tuning can be done modifying the angle of the chamfers or the waffle grid height.

Finally, the measured figures of directivity, gain and antenna efficiency are shown in Table II for four equispaced frequencies at broadside direction. Special mention deserve the measured efficiency values, over 94%, particularly remarkable for this 30 GHz targeted band. Such good results are consequence of the full-metallic waveguiding technology and the gap-waveguides capability to prevent field leakage. Notice, however, that directivity figures are from an integration of the measured full radiation pattern. Therefore, it is affected by the presence of the positioner and subjected to certain uncertainty in the tenths of dB. Obviously, antenna efficiency is also affected by this uncertainty. Also, it must be recalled that, as any corporate-fed array, efficiency values will decrease as aperture size becomes larger. Gain measurements has been carried out at the anechoic chamber facilities of Universidad Politécnica de Madrid, Spain, which are ISO-17025 standard certified.

TABLE II: Measured broadside antenna parameters.

Frequency (GHz)	29.5	30	30.5	31
Directivity (dBi)	21.94	22.18	22.3	22.44
Gain (dBi)	21.83	21.95	22.25	22.40
Antenna Efficiency (%)	97.5	94.84	98.9	99.1

VI. Conclusions

A 4 4 Ka-band single-layer circularly-polarized array of chamfered cylindrical apertures fed by gap waveguides has been presented. This antenna shows some singular characteristics. Low profile is attained as a result of integrating the circularly-polarized radiating element into the same layer as the feeding network. The concept can be seamlessly extended to a larger array without resorting to additional layers. This fact has been possible thanks to a novel feeding network topology combining groove and ridge-gap waveguides. Such a compact and easy-to-design network is capable of feeding coherently the proposed radiating apertures in a corporate way, without sacrificing the single-layer feature. Measurements give a good account of the design robustness because results are pretty consistent with simulations, regardless of some manufacturing errors detected. Measured antenna efficiency, along with pattern stability and good polarization performance, make the proposed low profile array architecture an attractive candidate for demanding SOTM applications.

References

[1] H. Zhou, M. Jong, and G. Lo, "Evolution of satellite communication antennas on mobile ground terminals," *International Journal of Antennas and Propagation*, vol. 2015, 2015.

[2] Y. Rahmat-Samii and A. C. Densmore, "Technology trends and challenges of antennas for satellite communication systems," *IEEE Transactions on Antennas and Propagation*, vol. 63, no. 4, pp. 1191–1204, April 2015.

[3] P. S. Kildal, E. Alfonso, A. Valero-Nogueira, and E. Rajo-Iglesias, "Local metamaterial-based waveguides in gaps between parallel metal plates," *IEEE Antennas and Wireless Propagation Letters*, vol. 8, pp. 84–87, 2009.

[4] A. Polemi, S. Maci, and P.-S. Kildal, "Dispersion characteristics of a metamaterial-based parallel-plate ridge gap waveguide realized by bed of nails," *IEEE Transactions on Antennas and Propagation,*, vol. 59, no. 3, pp. 904–913, March 2011.

[5] E. Rajo-Iglesias and P.-S. Kildal, "Groove gap waveguide: A rectangular waveguide between contactless metal plates enabled by parallel-plate cut-off," in *Proceedings of the Fourth European Conference on Antennas and Propagation (EuCAP), 2010*, April 2010, pp. 1–4.

[6] E. Pucci, A. Zaman, E. Rajo-Iglesias, and P.-S. Kildal, "New low loss inverted microstrip line using gap waveguide technology for slot antenna applications," in *Proceedings of the 5th European Conference on Antennas and Propagation (EUCAP)*, April 2011, pp. 979–982.

[7] A. Berenguer, M. Baquero-Escudero, D. Sanchez-Escuderos, B. Bernardo-Clemente, and V. E. Boria-Esbert, "Low insertion loss 61 ghz narrow-band filter implemented with groove gap waveguides," in *2014 44th European Microwave Conference*, Oct 2014, pp. 191–194.

[8] A. Berenguer, D. Snchez-Escuderos, B. Bernardo-Clemente, M. Baquero-Escudero, and V. E. Boria, "Groove gap waveguide as an alternative to rectangular waveguide for h-plane components," *Electronics Letters*, vol. 52, no. 11, pp. 939–941, 2016.

[9] A. Vosoogh, P. S. Kildal, and V. Vassilev, "Wideband and high-gain corporate-fed gap waveguide slot array antenna with etsi class ii radiation pattern in v -band," *IEEE Transactions on Antennas and Propagation*, vol. 65, no. 4, pp. 1823–1831, April 2017.

[10] J. Xi, B. Cao, H. Wang, and Y. Huang, "A novel 77 ghz circular polarization slot antenna using ridge gap waveguide technology," in *2015 Asia-Pacific Microwave Conference (APMC)*, vol. 3, Dec 2015, pp. 1–3.

[11] M. Ferrando-Rocher, A. Valero-Nogueira, and J. I. Herranz-Herruzo, "New feeding network topologies for high-gain single-layer slot array antennas using gap waveguide concept," in *2017 11th European Conference on Antennas and Propagation (EUCAP)*, March 2017, pp. 1654–1657.

[12] A. U. Zaman and P.-S. Kildal, "Gap waveguides," in *Handbook of Antenna Technologies*. Springer, 2016, pp. 3273–3347.

[13] M. Sano, J. Hirokawa, and M. Ando, "Single-layer corporate-feed slot array in the 60-ghz band using hollow rectangular coaxial lines," *IEEE Transactions on Antennas and Propagation*, vol. 62, no. 10, pp. 5068–5076, Oct 2014.

[14] D. Kim, M. Zhang, J. Hirokawa, and M. Ando, "Design and fabrication of a dual-polarization waveguide slot array antenna with high isolation and high antenna efficiency for the 60 ghz band," *IEEE Transactions on Antennas and Propagation*, vol. 62, no. 6, pp. 3019–3027, June 2014.

[15] E. Rajo-Iglesias and P. S. Kildal, "Groove gap waveguide: A rectangular waveguide between contactless metal plates enabled by parallel-plate cut-off," in *Proceedings of the Fourth European Conference on Antennas and Propagation*, April 2010, pp. 1–4.

[16] M. Ferrando-Rocher, A. U. Zaman, J. Yang, and A. Valero-Nogueira, "A dual-polarized slotted-waveguide antenna based on gap waveguide technology," in *2017 11th European Conference on Antennas and Propagation (EuCAP)*, March 2017, pp. 1–4.

[17] A. Jiménez, A. Valero-Nogueira, J. I. Herranz, and B. Bernardo, "Single-layer cavity-backed slot array fed by groove gap waveguide," *IEEE Antennas and Wireless Propagation Letters*, vol. 15, pp. 1402–1405, 2016.

[18] P. S. Kildal and M. N. M. Kehn, "The ridge gap waveguide as a wideband rectangular hard waveguide," in *Proceedings of the Fourth European Conference on Antennas and Propagation*, April 2010, pp. 1–4.